LIDAR SYSTEM SELF-CALIBRATION USING PLANAR PATCHES FROM PHOTOGRAMMETRIC DATA

Ayman F. Habib [a, *], Ki In Bang [a], Sung-Woong Shin [b], Edson Mitishita [c]

a Department of Geomatics Engineering, University of Calgary, Calgary, Alberta, Canada - (habib, kibang)@ucalgary.ca
b Spatial Information Research Team, Telematics & USN Research Division, Electronics and Telecommunications Research Institute, South Korea (sshin@etri.re.kr)
c Departamento de Geomática, Universidade Federal Do Paraná, Caixa Postal 19.001, 81.531-970 Curitiba, Paraná, Brasil (mitishita@ufpr.br)

KEY WORDS: Quality Assurance, System Biases, Linear Features, Areal Features, Surface Matching.

ABSTRACT:

The ever improving capabilities of the direct geo-referencing technology is having a positive impact on the widespread adoption of LIDAR systems for the acquisition of dense and accurate surface models over extended areas. Unlike photogrammetric techniques, derived footprints from a LIDAR system are not based on redundant measurements, which are manipulated in an adjustment procedure. The accuracy of derived LIDAR footprints depends on the quality of the bore-sighting parameters among the system components: namely, the laser, GPS, and INS units. Current methodologies for estimating the bore-sighting parameters of a LIDAR system are based on complicated and sequential calibration procedures. This paper presents a new methodology for estimating the LIDAR bore-sighting parameters through a tight integration procedure that involves photogrammetric data and raw measurements from a LIDAR system. Then, the LIDAR bore-sighting parameters are determined by minimizing the normal distances between the derived LIDAR footprints and the photogrammetric patches. The whole procedure is implemented in an integrated bundle adjustment that incorporates the photogrammetric data as well as the raw LIDAR measurements. An analysis will be conducted to determine the optimum configuration of the control patches as well as the flight pattern for reliable estimation of the bore-sighting parameters while avoiding possible correlations. Besides the estimation of the bore-sighting parameters, the proposed methodology will also ensure the co-registration of the photogrammetric and LIDAR data to a common reference frame, which will have a positive impact on further products such as orthophotos and generated photo-realistic 3D models. The findings of the conducted analysis will be verified through experimental results from simulated data.

1. INTRODUCTION

A typical LIDAR system consists of three main components, a GPS system to provide position information, an INS unit for attitude determination, and a LASER system to provide range (distance) information between the LASER firing point and the ground point. In addition to range data, modern LIDAR systems can capture intensity images over the mapped area. Therefore, LIDAR is being more extensively used in mapping and GIS applications.

Figure 1 shows an example of a schematic diagram of a LIDAR system together with the involved coordinate systems. Equation 1 is the basic LIDAR geometric model that incorporates the LIDAR measurements for deriving positional information (El-Sheimy et al., 2005). This equation relates four coordinate systems, which include the ground coordinate system, the inertial navigation system (INS) body frame coordinate system, the laser unit coordinate system, and the laser beam coordinate system. This equation is simply the result of three vectors summation; $\overrightarrow{X_0}$ is the vector from the origin of the ground coordinate system to the GPS antenna phase center, $\overrightarrow{P_G}$ is the offset between the laser unit and the GPS phase center with respect to the laser unit coordinate system, and ρ is the measured distance between the laser beam firing point and the target point. The summation of these three vectors after applying the appropriate rotations ($R_{\omega,\phi,\kappa}, R_{\Delta\omega,\Delta\phi,\Delta\kappa}, R_{\alpha,\beta}$) will yield the vector $\overrightarrow{X_G}$, which represents the ground coordinates of the object point under consideration. The quality of the derived surface depends on the accuracy of the involved sub-systems (i.e., laser, GPS, and INS) and the calibration parameters relating these components (i.e., bore-sighting parameters).

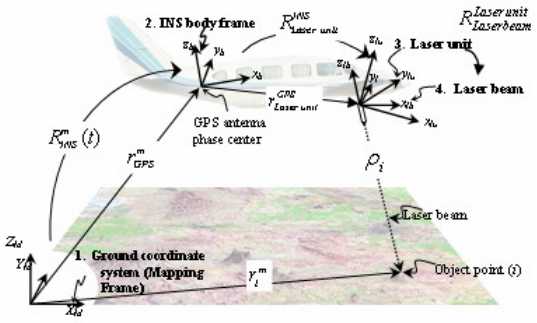

Figure 1. Coordinates and parameters involved in a LIDAR acquisition system

* Corresponding author.

$$\vec{X}_G = \vec{X}_o + R_{\omega,\phi,\kappa}\, R_{\Delta\omega,\Delta\phi,\Delta\kappa}\, \vec{P}_G + R_{\omega,\phi,\kappa}\, R_{\Delta\omega,\Delta\phi,\Delta\kappa}\, R_{\alpha,\beta} \begin{bmatrix} 0 \\ 0 \\ -\rho \end{bmatrix} \quad (1)$$

Even though the individual measurement capabilities of the system components (GNSS, INS and laser scanner system) are quite precise, serious errors can occur from inaccurate combination of theses components. For this reason, bore-sighting parameters should be well defined in the beginning of the work process. The calibration of a LIDAR system is a complex task. The ultimate goal is to determine all systematic errors and to correct the raw laser measurements such that only random errors remain. The calibration proceeds through several steps, beginning with calibrating individual system components in the laboratory, followed by a system calibration on the platform (mounting parameters), and in-situ calibrations before and after the mission (Schenk 2001).

Prior research has addressed the analysis and calibration of the LIDAR system errors. The sources of the systematic errors, which can occur in a LIDAR system, have been previously analyzed together with their impact on the derived surface (Schenk, 2001; Habib et al., 2006). In addition, an attempt for system parameter estimation has been carried out by Schenk (2001), where some of the system parameters are individually estimated, while others, due correlation, are determined as a group. Morin (2002) introduced a calibration methodology using overlapping strips, where the bore-sight misalignment and scanner torsion are estimated via least squares adjustment involving the LIDAR measurements. Filin (2003) tried to correct the system parameters using natural surfaces to determine the mounting and the range biases. In industry, the approach taken by Hanjin (2006) is more closely applicable in practice. To calibrate the LIDAR system, a calibration field, which is composed of well-known surfaces, is devised. Using the calibration site, discrepancies between the LIDAR point cloud and the reference surface are observed and used to determine the system parameters such as the bore-sighting roll and pitch angles and scale parameters (Hanjin 2006).

Some of the existing calibration methods involve manual and empirical procedures, and some have limitations in terms of which parameters can be determined through the calibration process. In this paper, the error sources are analyzed and an alternative method is proposed for the system calibration. More specifically, a method using the LIDAR raw measurements is introduced, and a multi-sensor triangulation, which is developed for the integration of LIDAR and photogrammetric data, is proposed. Planar patches are used as the control data. Using control planar patches is advantageous for several reasons. For instance, planar patches are easy to collect from the photogrammetric data and LIDAR point cloud. Moreover, man-made environments are rich with such primitives.

The following section gives an analysis of the LIDAR error budget, and Section 3 presents the proposed methodology for system calibration as well as the optimal configuration of the control patches and flight pattern. Experimental results from a simulated data will be introduced in the same section. Finally, conclusions and recommendation for future research will be summarized.

2. ERROR BUDGET OF A LIDAR SYSTEM

As mentioned before, the error in the LIDAR-derived coordinates is affected by errors in the components of the LIDAR system. These components, or input parameters, can either be estimated or measured from a system calibration procedure. In this section, we are interested in analyzing the effect of random noise and systematic biases in the measurements from the various LIDAR components on the final product. The purpose of such analysis is to allow for the estimation of the quality of the final product in terms of the quality of the system's measurement. Moreover, knowing the expected accuracy of the final product, one might be able to interpret the outcome of the quality control procedure as being acceptable or as an indication of the presence of systematic biases in the data acquisition system. Finally, by analyzing the effect of systematic biases, one might be able to offer some diagnostic tips about the origin of identified discrepancies from the proposed quality control procedures.

For any point measured by the LIDAR system, error propagation can be used to determine the error in the LIDAR-derived coordinates given the errors in the LIDAR input parameters. It should be noted that the error budget does not consider the effect of LIDAR interaction with different terrain and ground cover types. In other words, the error budget assumes a relatively flat solid surface. To facilitate the estimation of the contribution of error sources in various LIDAR components to the final accuracy of the derived point cloud, an error propagation calculator has been devised. The calculator allows the user to specify values for each of the system input parameters for a certain LIDAR footprint, and to enter the noise level for each of the parameters. The calculator then determines the accuracy of the ground coordinates of the point. Conversely, if the user requires specific accuracy for the final ground coordinates, the calculator can be used to determine the accuracies that would be required for the input components through a trial and error process.

Figure 2 shows the calculator's user interface. In this figure, sample typical values for the LIDAR input parameters have been entered along with the sigma values. The output box gives the variance-covariance matrix of the final ground coordinates of the point in question, followed by the respective standard deviations. Using such a calculator, one can answer the following questions:

- What is the error budget for each source component in the LIDAR equation?
- What is the best possible achievable accuracy for a given LIDAR component configuration based on the manufacturer's standard deviations?

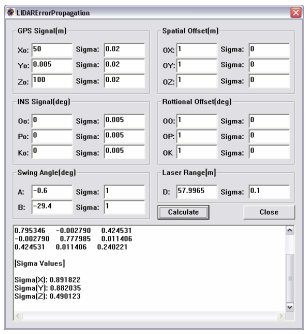

Figure 2. Error propagation calculator

Another related issue to the LIDAR error analysis is the nature of resulting errors from random errors in the input system measurements. Usually, it is expected that random noise will lead to random errors in the derived point cloud. Moreover, it is commonly believed that random noise will not affect the relative accuracy. However, this is not the case for LIDAR systems. In other words, some of the random errors might affect the relative accuracy of the derived point cloud. Depending on the considered parameter, the relative effect of the corresponding noise level might not be the same. As an illustration, Figure 3 shows that a given attitude noise in the INS derived orientation will affect the nadir region of the flight trajectory less significantly than off nadir regions. Thus, the INS error will affect the relative accuracy of LIDAR derived point cloud. The following list gives some diagnostic hints about the impact of noise in the system measurements on the derived point cloud.

- GPS noise: It will lead to similar noise level in the derived point cloud. Moreover, the effect is independent of the system parameters (flying height and look angle).
- Angular noise (INS or mirror angles): For this type of noise, the horizontal coordinates are affected more than the vertical coordinates. In addition, the effect is dependent on the system parameters (flying height and look angle).
- Range noise: It mainly affects the vertical component. The effect is independent of the system flying height. However, the impact is dependent on the system look angle.

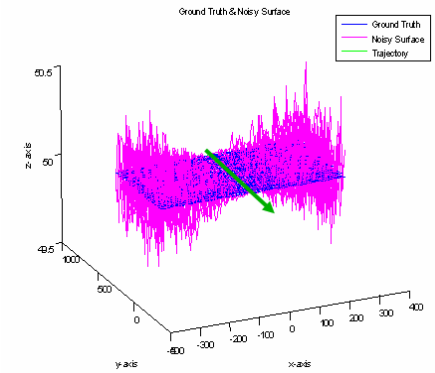

Figure 3. The effect of attitude error on a simulated horizon surface

	Flying Height	Flying Direction	Look Angle
Bore-sighting Offset Bias	Effect is independent of the Flying Height	Effect is dependent on the Flying Direction (Except ΔZ)	Effect is independent of the Look Angle
Bore-sighting Angular Bias	Effect Increases with the Flying Height	Effect Changes with the Flying Direction	Effect Changes with the Look Angle (Except ΔX)
Ranging Bias	Effect is independent of the Flying Height	Effect is independent of the Flying Direction	Effect Depends on the Look Angle (Except ΔY)
Scan angle Bias	Effect Increases with the Flying Height	Effect Changes with the Flying Direction (Except ΔY)	Effect Changes with the Look Angle (Except ΔX)

Table 1. Systematic biases and their impact on the derived surface with linear scanner system, flat horizontal terrain, and straight trajectory along the Y-direction and constant attitude

Systematic biases in the system measurements (e.g. GPS/INS measurements, mirror angle measurements, measured ranges) and calibration parameters (e.g. bore-sighting parameters relating the system components) will lead to systematic errors in the derived point cloud. Table 1 provides a summary of the various systematic biases and their impact on the derived LIDR coordinates.

3. LIDAR SYSTEM CALIBARTION

For a system calibration, control information is essential. Traditionally, distinct control points have been used for the calibration of photogrammetric systems. One of the key characteristics of LIDAR data is the irregularity of the derived point cloud. While LIDAR data provides very accurate three-dimensional positional information, its visual information is not enough to extract distinct points (Figure 4). For example, it is nearly impossible to identify the laser footprint in the corresponding images (Ghanma 2006). For this reason, using control planar patches is easier and more effective for the LIDAR system calibration. In this research, we propose the integration of photogrammetric and LIDAR data for LIDAR system calibration. The photogrammetric data will be used to provide the necessary control planar patches for LIDAR calibration.

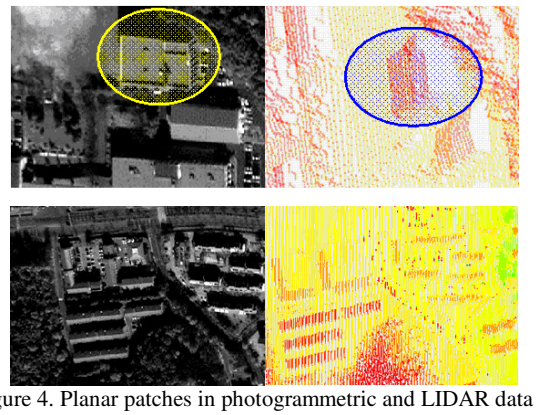

Figure 4. Planar patches in photogrammetric and LIDAR data

Using control patches, we can determine the LIDAR parameters that minimize the normal distance between the laser footprints and the corresponding control patches. Control planar patches can be derived from photogrammetric data such as aerial photos and satellite images. For example, we can observe three corner points on the plane from overlapping images and the corresponding object coordinates of these points are calculated through a bundle adjustment procedure. As previously mentioned, a LIDAR system generally has four kinds of observations. These include GNSS observations for the positional information, INS observations for the platform attitude determination, scan angles of the laser beam, and distances between the laser firing point and the object surface. We must also consider the bore-sighting parameters: spatial and rotational offset values between the origins of GNSS/INS and the laser unit coordinate system. In this research, LIDAR system calibration mainly focuses on these bore-sighting parameters. In the remainder of this paper, the feasibility of using planar patches derived from photogrammetric data for the LIDAR calibration is discussed.

In this research, the photogrammetric bundle adjustment is augmented by adding the LIDAR geometric model to the collinearity equation for the LIDAR system calibration. The collinearity equations are introduced in Equation 2, where the image and object coordinates of the planar patches are related to the interior and exterior orientation parameters of the imaging system. In this equation, the object coordinates of the vertex points, which are identified in overlapping images, are unknowns.

$$F_{I_x} = x - x_p = -f\frac{m_{11}(X_v - X_0) + m_{12}(Y_v - Y_0) + m_{13}(Z_v - Z_0)}{m_{31}(X_v - X_0) + m_{32}(Y_v - Y_0) + m_{33}(Z_v - Z_0)} = -f\frac{r}{q} \quad (2)$$

$$F_{I_y} = y - y_p = -f\frac{m_{21}(X_v - X_0) + m_{22}(Y_v - Y_0) + m_{23}(Z_v - Z_0)}{m_{31}(X_v - X_0) + m_{32}(Y_v - Y_0) + m_{33}(Z_v - Z_0)} = -f\frac{s}{q}$$

where ω, ϕ, κ, X_O, Y_O, and Z_O are the exterior orientation parameters of the imaging sensor,

f, x_p, y_p are the interior orientation parameters of the imaging sensor,

$P_{vertex} = (X_v, Y_v, Z_v)$ are the coordinates of a vertex point, and

$p = (x, y)$ are the coordinates of the corresponding image point.

m_{ij} are the elements of the rotation matrix(M)

In Figure 5, A, B, and C denote vertex points of a planar patch, which is defined by the photogrammetric data. A LIDAR point that belongs to this planar patch is denoted by G_i. A well calibrated LIDAR system should produce a point that has a normal distance to the plane that is close to zero. In other words, the volume of the triangular pyramid which consists of the four points A, B, C, and G_i should be zero.

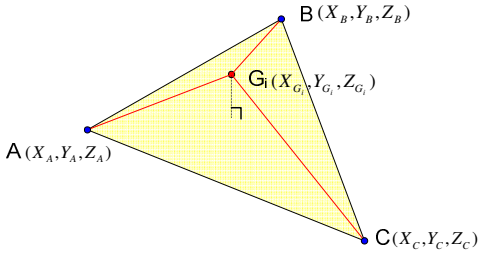

Figure 5. Triangular constraint between a LIDAR point G_i and a planar patch represented by A, B, and C

The volume of the triangular pyramid can be calculated by Equation 3, and the LIDAR point, G_i, can be obtained by LIDAR geometric model (Equation 1) using LIDAR raw measurements. The unknowns in Equation 3 include the ground coordinates of the photogrammetric patch together with the LIDAR bore-sighting parameters.

$$V = \begin{vmatrix} X_{G_i} & Y_{G_i} & Z_{G_i} & 1 \\ X_A & Y_A & Z_A & 1 \\ X_B & Y_B & Z_B & 1 \\ X_C & Y_C & Z_C & 1 \end{vmatrix} \times \frac{1}{6} = 0 \quad (3)$$

where $(X_{G_i}, Y_{G_i}, Z_{G_i})$ = LIDAR point LIDAR point

$\{(X_A, Y_A, Z_A), (X_B, X_B, X_B), (X_B, X_B, X_B)\}$ = vertex points

Using distinct control points, the geo-referencing parameters of the involved imagery can be indirectly estimated, which can be simultaneously used to derive the ground coordinates of the control patch. Alternatively, an integrated GPS/INS unit can be used to directly geo-reference the involved imagery. The comparative analysis between the performance of direct and indirect geo-referencing procedures will be evaluated in the experimental results section. On the other hand, the next section deals with the optimum configuration for reliable estimate of the bore-sighting parameters.

3.1 Optimal Configuration of the Control Patches & Flight Plan

To ensure reliable estimation of the bore-sighting parameters, one must investigate the optimum configuration of the control patches together with flight pattern. An optimum configuration is the one that yields an accurate estimate of the parameters while avoiding any possible correlations. For the control patches, the ideal configuration is shown in Figure 6.a. In other words, orthogonal patches in the XY, XZ, and YZ-planes are desired. However, this situation is not realistic (i.e., it is not always guaranteed that such a configuration can be available).

A more realistic planar patch configuration is shown in Figure 6.b. For this configuration, horizontal and sloping planar patches are used for the calibration process. It is important to have sloping planar patches with different aspects (e.g., some of the patches can be parallel to the X-axis while others are parallel to the Y-axis).

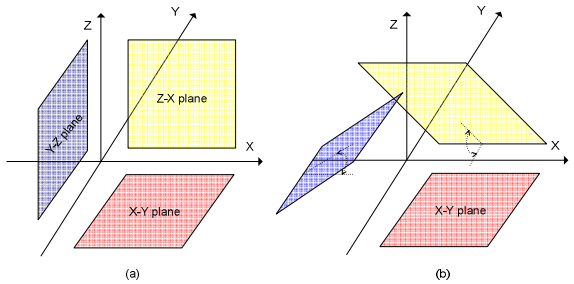

Figure 6. Optimal (a) and realistic (b) planar patches for the LIDAR system calibration

To test the performance of this configuration together with the impact of the slope of such patches, we simulated a LIDAR strip using a linear scanner system at 1500 m flying height with 25 deg scan angle. The simulation process starts with a surface model and system trajectory. Using such information, we derived the LIDAR measurements, which are then used to estimate the bore-sighting parameters through the proposed methodology in the previous section. The estimated bore-sighting parameters are then used to reconstruct the surface. Finally, root mean square error analysis (RMSE) is used to compare the original and reconstructed surfaces. The conducted tests for this experiment utilize control patches, which are readily available (i.e., for these tests, we directly use control patches for LIDAR calibration).

The performance of the calibration process while considering LIDAR and photogrammetric data will be discussed in section 4. Figure 7 shows the accuracy of the reconstructed coordinates using the recovered bore-sighting parameters from five well-distributed control patches along the LIDAR swath with varying slopes. Figure 8 shows the discrepancies between the true bore-sighting parameters and recovered ones. As it can be seen in Figure 7 and Figure 8, if the slope of the planes is very small (e.g., less than 10 deg), the three planar patches are almost

parallel, and the RMSE of the reconstructed coordinates of LIDAR points are very high. It is also seen that for such a case, the derived bore-sighting parameters are not close to the true parameters. Therefore, it is recommended that some of the control patches should have slopes that exceed 10 degrees. Moreover, the patches should have different orientation in space (i.e., different aspect angles).

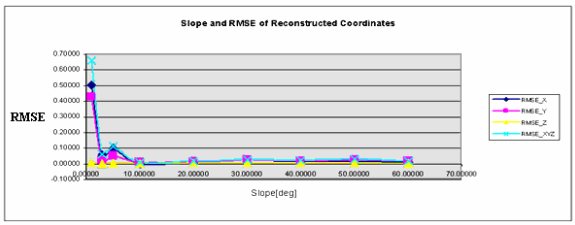

Figure 7. Slope of planar patches and accuracies of reconstructed surface

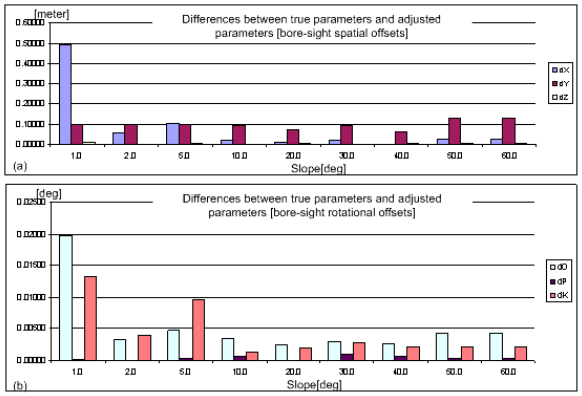

Figure 8. Differences between true bore-sighting parameters and derived ones

Before the calibration, we need to analyze the error coming from each system parameter that is related to the LIDAR calibration. In particular, the errors in the bore-sighting parameters significantly affect the final positions of LIDAR points. This paper defines ω_{bias}, ϕ_{bias} and κ_{bias} as errors in the rotational bore-sighting offset and ΔX, ΔY and ΔZ as errors in the bore-sighting spatial offset with respect to the GNSS/INS coordinate system. One of the significant difficulties in system calibration is that some parameters' correlations are high. The following discussion explains the correlation problems and how to avoid this problem. First, to simplify the problem, we assume flat terrain and constant platform attitude. Under this idealized condition, the rotational bore-sighting offset error ω_{bias} and bore-sighting spatial offset error ΔY are tightly coupled with each other.

Figure 9 show the errors in ground coordinates for one cycle (or scan) of data, whose errors are due to spatial offset (ΔX, ΔY and ΔZ), angular offset ω_{bias} in a linear scanner system and elliptical scanner system, respectively. The X axis represents the location of the point along the scan line and the Y axis of the figure displays the differences, in meters, between true coordinates and distorted coordinates resulting from the offset errors. As shown in Figure 9.a, bore-sighting spatial offset values generate constant errors on the ground. And the effect of the spatial offset is same in the both system: linear scanner system and elliptical scanner system, because the effect of the spatial bore-sighting offset on the ground coordinates is independent of the scan angles as shown in the LIDAR system geometric model. On the other hand, angular offset ω_{bias} produces different error patterns in both systems. In Figure 9.b, the error graph of linear scanner system shows the constant errors like the error pattern of spatial offset and the error pattern of ω_{bias} in the elliptical scanner system is different from the case of the linear scanner system.

The point to which we give attention in these graphs is to the pattern effect of the error due to angular offset (Figure 9.b and Figure 9.c), which is seen to be similar to the pattern in Figure 9.a, which shows the error effect due to spatial offsets. This means that angular offsets can be correlated with spatial offsets.

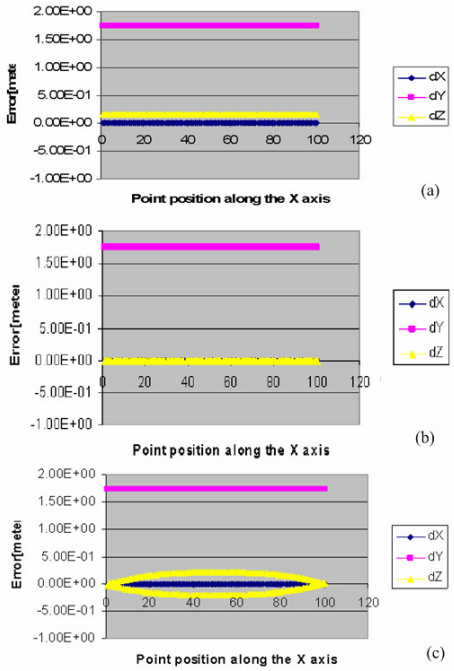

Figure 9. Error patterns occurred by bore-sighting spatial offsets, ΔX, ΔY and ΔZ, in linear and elliptical scanner system (a), bore-sighting rotational offset, ω_{bias}, in linear scanner system (b), and bore-sighting rotational offset, ω_{bias}, in elliptical scanner system (c)

In the elliptical scanner system, to avoid the correlation between ω_{bias} and ΔY, we should ensure that the maximum error ($dZ_{\max}$) in the Z coordinates is larger than the size of the random error (Figure 10). If this value is not larger than the size of the random error, this curved error pattern caused by the effect of the rotational bore-sighting offset error ω_{bias} can not be distinguished from the constant error pattern caused by the effect of the spatial bore-sighting offset error ΔY. Using Equation 4 which is derived form the LIDAR geometric model (Equation 1), we can calculate the optimal flying height to avoid the correlation between ω_{bias} and ΔY in the elliptical scanner system.

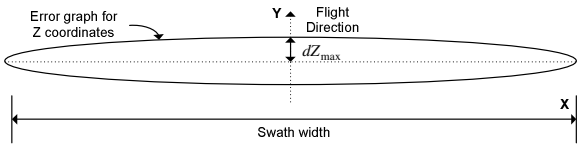

Figure 10. *Z* coordinate error pattern caused by ω_{bias} along the scan line in elliptical scanner system

$$H_{opt} = \frac{dZ_{\max}(> e_{rand})}{(1+\sin\omega_{bias}\tan\alpha_T - \cos\omega_{bias})} \quad (4)$$

where e_{rand} is size of random error, and
H_{opt} is optimal flying height from the ground.

More significant correlation can be occurred in the linear scanner system. As shown in Figure 9.a and 9.c, rotational bore-sighting offset ω_{bias} produce constant errors, and this error pattern look like errors caused by spatial bore-sighting offset. The spatial bore-sighting offset produces the same errors in ground coordinate even when the swath width is changed by using different flying height and different scan angles. On the other hand, errors introduced by rotational bore-sighting offset change for different flying heights or scan angles. For this reason, we can avoid the correlation in the linear scanner system when we use at least two different overlap strips, which are captured by using two different strips captured at different flying heights. The optimal flying height difference between two strips can be obtained when the size of the *Y* coordinate difference between two different strips is large than the size of the random error and Equation 5 represents a formula used in calculating the optimal flying height difference.

$$\frac{dY(> e_{rand})}{-\sin\omega_{bias}} = dH_{opt} \quad (5)$$

where dY is a maximum *Y* coordinate difference between two different strips, and
dH_{opt} is optimal flying height from the ground.

A similar situation can occur for an angular offset ϕ_{bias} and a spatial offset ΔX. Figure 11 shows the error pattern caused by the rotational bore-sighting offset error ϕ_{bias} in the linear scanner (Figure 11.a) and the elliptical scanner (Figure 11.b). The difference of this error pattern in comparison with the error pattern caused by the spatial bore-sighting offset errors (constant errors) is most significant in the values of dZ. Therefore, we have to be sure that $dZ_{\max}$ is larger than the random error size (Figure 12). The optimal flying height to avoid the correlation can be obtained by Equation 6.

3.2 Optimal Flight Plan Test

For the investigation of the optimal flight plan, thirteen configurations are tested (refer to Table 2 for the specifications of such flight plans). Tests 1 and 2 use only a single strip, Tests 3 ~ 8 use two strips with different flying directions but with the same flying height, and Tests 9 ~ 13 involve two or three strip with different flying heights and different flying directions. In addition, Test 8 has two strips with 75% overlap.

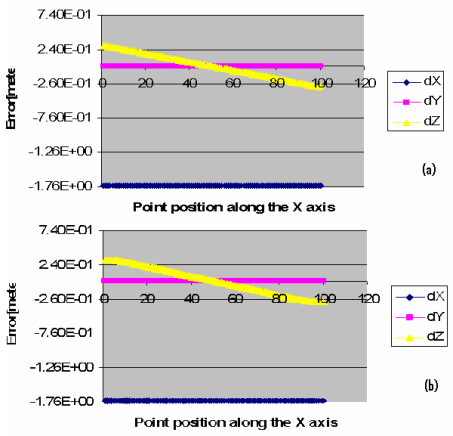

Figure 11. Error patterns occurred by bore-sighting rotational offset ϕ_{bias} in linear scanner system (a), and elliptical scanner system (b)

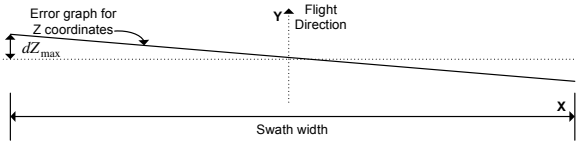

Figure 12. *Z* coordinate error pattern caused by ϕ_{bias} along the scan line in linear scanner system

$$H_{opt} = \frac{dZ_{\max}}{\sin\phi_{bias}\tan\beta_T + (1-\cos\phi_{bias})} \quad (6)$$

where β_T is an total angular field of view of the laser scanner around flight direction.

No #	Test 1	2	3	4	5	6
Flying direction & Flying height	S2N 500m	E2W 1500m	S2N 2500m E2W 2500m	S2N 500m N2S 500m	S2N 2500m N2S 2500m	E2W 500m S2N 500m
Overlap	N/A	N/A	100%	100%	100%	100%
Flying height	500m	1500m	2500	500m	2500	500m 500m
*TAFOV	40deg					
Scan rate	200Hz					
Laser pulse rate	33.33 kHz					

No #	Test 7	8	9	10	11	12	13
Flying direction & Flying height	S2N 2500m N2S 2500m	S2N 2500m N2S 2500m	S2N 500m S2N 1500m	S2N 500m S2N 2500m	S2N 500m S2N 1500m S2N 2500m	E2W 500m S2N 2500m	E2W 2500m S2N 500m
Overlap	100%	75%	100%	100%	100%	100%	100%
Flying height	2500m 2500m	2500m 2500m	500m 1500m	500m 2500m	500m 1500m 2500m	500m 2500m	2500m 500m
Trajectory	Constant velocity and attitudes						
GNSS random error	±5cm						
INS random error	±0.005deg						
*TAFOV	40deg						
Scan rate	200Hz						
Laser pulse rate	33.33 kHz						

Table 2. Description of the flight patterns for the LIDAR calibration (*TAFOV: Total Angular Field Of View)

For the calibration, 25 patches are used for each strip and these planar patches are simulated under the above mentioned optimal

configuration. Each planar patch is a right-angled triangle of which each side is 5.0m while the slopes range from 0 deg (parallel to ground) to 30 deg (for the tilted patches). There are two kinds of tilted patches, one is parallel to the X axis and the other is parallel to Y axis. It can be seen that they are regularly distributed throughout the scanned area.

Figure 13 shows the RMSE of the reconstructed coordinates of LIDAR points using the estimated bore-sighting parameters from the various tests. The random errors in the simulated test data are about ±5 cm for GNSS position and ±0.005deg for the INS orientation (which is equivalent to ±22cm at a flying height of 2500m). The RMSE of the reconstructed coordinates using the estimated bores-sighting parameters from the various tests are smaller than these random errors for all the flight patterns. These results were proven by the slope tests above, where it was seen that for a slope greater than 20 deg and a good distribution of planar patches, the RMSE are smaller than the size of the random errors, Figure 13.

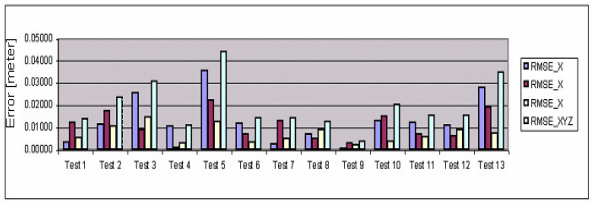

Figure 13. RMSE of reconstructed coordinates of LIDAR points under different flight patterns

However, we need to give attention to Figure 14, which shows the differences between the derived bore-sighting parameters and the true ones. Even though the RMSE of the reconstructed coordinates of the LIDAR points are smaller than the size of system random errors, the accuracy of the derived parameters might not be good enough to recover the ground coordinates of the LIDAR points under different flying configurations.

In summary, horizontal and sloping planar patches are essential for reliable estimation of the bore-sighting parameters. Moreover, the flight pattern of the LIDAR system plays a significant role. It is preferred to have two overlapping strips from two different flying heights (refer to experiments 9 – 13). In addition, flying in cross and/or opposite strips will lead to slightly better results. Having established the feasibility of using control patches for LIDAR calibration, the focus will be shifted towards the analysis of the integration of photogrammetric and LIDAR data while considering direct and indirect geo-referencing alternatives.

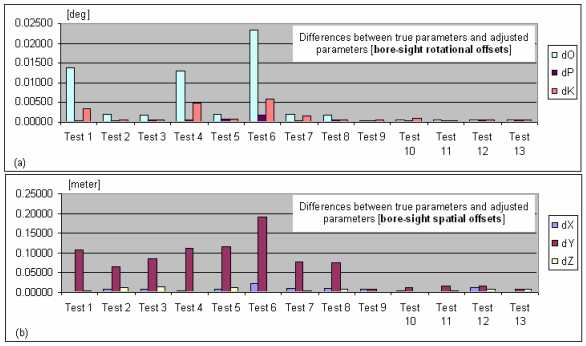

Figure 14. Differences between true and estimated bore-sighting parameters from different flight patterns

4. BUNDLE ADJUSTMENT FOR LIDAR CALIBRATION

The following tests deal with photogrammetric data as well as LIDAR point cloud with the planar patches derived from photogrammetric intersection using bundle adjustment. The test data used contains two overlapping photos and two LIDAR strips from different flying heights. The photogrammetric geo-referencing is indirectly established using few ground control points (GCPs) or directly derived from an onboard GNSS/INS unit. For the indirect geo-referencing, 12 tie points and 4 GCPs are used, and for the direct geo-referencing 16 tie points and GNSS/INS data are used. Table 3 shows the simulation parameters for the photogrammetric data. For the LIDAR simulation, two different flying heights, 500m and 2,500m, are used with parallel flying directions in order to avoid correlation between the bore-sighting parameters.

Table 4 to Table 7 show the result and quality of the LIDAR calibration using simulation data under the above conditions. The first test has two strips with parallel flight directions and different flying heights, for which the image geo-referencing is performed indirectly (see Table 4 and Table 5). The second test is identical to the first one; with the exception that the image geo-referencing is performed directly (see Table 6 and Table 7). Table 4 and Table 6 show the result of the calibration and recovered bore-sighting parameters. A check strip is chosen in order to check the accuracy of the recovered parameters. This check strips is chosen to have a different flying height than those used in the calibration, but which covers the same area. Table 5 and Table 7 show the RMSE of the reconstructed LIDAR footprints in this strip. The check strip has a flying height of 1500m and is generated by a linear LIDAR system over the same area. It is clearly evident that the direct and indirect geo-referencing of the involved imagery yield comparable results.

Item	Descriptions
Overlap rate	About 60%
Image Size	9"x 9"
Focal length	150mm
Flying height	2500m
Image point measurement errors	-5um ~ +5um
GCP precision (indirect geo-referencing)	-5cm ~ +5cm
INS precision (direct geo-referencing)	-0.008deg~ +0.008deg
GNSS precision (direct geo-referencing)	-10cm ~ +10cm

Table 3. Description of the simulation parameters of the photogrammetric data

σ	5.92E-01	
Xb(M)	Yb(M)	Zb(M)
3.9713371474e-4	-3.2689161448e-3	3.1413554246e-5
Ob(deg)	Pb(deg)	Kb(deg)
5.0412193483e-4	2.5096596059e-4	1.2095043584e-3

Table 4. LIDAR calibration with bundle adjustment (Test A: Indirect geo-referencing case)

RMSE_X[M]	RMSE_Y[M]	RMSE_Z[M]
6. 0649805475e-03	1. 0958787364e-02	1. 2618518246e-03

Table 5. Surface reconstruction result for the check strip (Test A: Indirect geo-referencing case)

σ	5.92E-01	
Xb(M)	Yb(M)	Zb(M)
3.9713371453e-4	-3.2689161421e-3	3.1413554248e-5
Ob(deg)	Pb(deg)	Kb(deg)
5.0412193485e-4	2.5096596057e-4	1.2095043588e-3

Table 6. LIDAR calibration with bundle adjustment (Test B: Direct geo-referencing case)

RMSE_X[M]	RMSE_Y[M]	RMSE_Z[M]
6. 0649805472e-03	1. 0958787365e-02	1. 2618518245e-03

Table 7. Surface reconstruction result for the check strip (Test B: Direct geo-referencing case)

This experiment addresses the feasibility of the photogrammetric data integration with LIDAR raw data for LIDAR system calibration. By using the imagery data for the LIDAR calibration, we can reduce the quantity of ground control patches that are required, and have a good distribution of the control patches over the whole area that is covered by the LIDAR data and the imagery. In summary, the conclusion that can be drawn is that LIDAR calibration can be done using the integration of raw LIDAR data in a photogrammetric bundle adjustment. The advantage of this procedure is that it allows for a cost effective calibration method without the need for ground surveying of the control planar patches.

5. CONCLUSIONS

This paper addresses a new method for LIDAR system calibration while using raw LIDAR data. It has been established that the bore-sighting parameters can cause serious errors if their accuracy is not good enough. Control planar patches were used since ground control points which are traditionally used for the photogrammetric data are not distinguishable in irregular points such as those provided by a LIDAR system. In this work, photogrammetric data is used to derive the control patches, which are simultaneously incorporated for the calibration of the LIDAR system. In addition to the mathematical model for the LIDAR system calibration, the optimal configurations for the flight conditions and the distribution of planar patches have also been discussed.

As shown in the results of the calibration tests, we can recover the bore-sighting parameters using two strips with different flying heights. It is worth noting that in order to recover the correct bore-sighting parameters under varying conditions; we have to avoid any correlation between the rotational and spatial bore-sighting parameters. These correlations distort the system parameters, and thus even though the quality of the ground reconstruction is accurate for one case, these distorted parameters might negatively affect the reconstructed ground coordinate accuracy if used for strips which are captured with different flight condition (e.g., different flying heights and/or different scan angles). Finally, the bundle adjustment with raw LIDAR data successfully recovers the bore-sighting parameters and this quality is as good as the case of LIDAR calibration with control patches observed by field surveying. The success that has been achieved in this challenging issue opens the door to new possibilities for the development of effective calibration methods such as an automated procedure for the calibration, in addition to offering a cost effective method for LIDAR data quality assurance. Current research is focusing on verifying these results by using real data.

Acknowledgement

This research work has been conducted with partial funding from the GEOIDE Research Network (SII 43). The authors are grateful for Terrapoint Canada Inc. for the valuable feedback.

REFERENCES

Brenner, C.(2006), Aerial Laser Scanning, International Summer School "Dital Recording and 3D Modeling", ISPRS commission VI Special Interest Group "Technology Transfer Caravan", Crete, Greece

El-Sheimy N., Valeo, C., Habib, A., 2005. Digital Terrain Modeling: Acquisition, Manipulation And Applications, Artech House Remote Sensing Library, 200 pages.

Ghannma, M.(2006), Integration of Photogrammetry and LIDAR, Ph.D. thesis, University of Calgary

Filin, S.(2003), Recovery of Systematic Biases in Laser Altimetry Data Using Natural Surfaces, PE&RS, Vol. 69, No. 11

Habib, A., Jennifer Lay, Carmen Wong (2006), Specifications for the Quality Assurance And Quality Control of LIDAR Systems, Geomatics Engineering UofC

Hanjin Information System & Telecommunication Co., Ltd (2006), Computing Determinant method for Calibrating Airbornelaser Surveying System, Patent Document (http://patent2.kipris.or.kr/patent/KP/KPDI1010.jsp#Book10)

Morin, K.W.(2002), Calibration of Airborne Laser Scanners, M.S. thesis, Geomatics Engineering UofC

Optech, ALTM Technical Overview (2006) http://www.optech.ca/altmhow.htm

Schenk, T.(2001), Modeling and Analyzing Systematic Errors in Airborne Laser Scanners, the Ohio Sate University